ORIGINAL PAPER

Interactive Phenomena of a Rotating Arc and a Premixed CH$_4$ Flame

Nakyung Hwang · Jongguen Lee · Dae Hoon Lee · Young-Hoon Song

Abstract The interactive phenomena between a rotating arc and a premixed methane/air flame have been investigated. The effects of the rotating arc on the flame were observed: both lean and rich flammability limit was extended with the rotating arc on. More interestingly, the opposite interactions, i.e., the effects of the flame on the rotating arc, were also observed: the arc length, angular speed, and electrical characteristics are affected by the flame. An analysis of the optical emission spectra showed that the rotating arc generates chemically active species such as excited N$_2$ molecules and O and H atoms. An analysis of the gas products indicated that the concentrations of the major gas products such as CO$_2$, CO, and H$_2$ were not significantly affected by the rotating arc, although the flammability limit are significantly extended. Unlike these major gas products, minor products like NO$_x$ emissions increased by an order of magnitude in the presence of a rotating arc under certain air/fuel conditions.

Keywords Plasma · Combustion · Premixed flame · Interaction · Rotating arc

Introduction

Plasma has been utilized to stabilize and ignite flames under the harsh conditions, e.g. extremely lean burn combustion [1–3], diesel combustion in a diesel exhaust line for regenerating DPF (Diesel Particulate Filter) [4]. In such applications of plasma, the roles of the plasma are diverse; generating the chemically active species such as electrons, radicals, excited molecules [5–9], supplying thermal heat to combustion reactions [10, 11], providing combustible H$_2$ and CO gases to the flames through plasma fuel reforming process

N. Hwang · D. H. Lee · Y.-H. Song (✉)
Green Environmental System Research Department, Korea Institute of Machinery and Materials,
171 Jang-dong, Yusong-gu, Daejeon 305-343, Korea
e-mail: yhsong@kimm.re.kr

J. Lee
Department of Mechanical and Nuclear Engineering, Pennsylvania State University, 135 Research
Building East, University Park, PA 16802, USA

[1, 3], etc. Recently, among the numerous techniques of plasma generation, gliding or rotating arc discharges have been suggested as one of the practical techniques for chemical processes, especially for fuel reforming process [12–18]. These gliding or rotating arc discharges are typically generated by relatively high voltage (few kV) and low current (order of mA) conditions. The previous fundamental studies on the gliding arc have revealed that the arc is classified as non-equilibrium plasma in which the electron temperature is much higher than that of ions or neutral molecules [19–24]. The geometrical configurations of gliding or rotating arc reactors are simple, and this makes its application to combustion devices easier.

Although gliding or rotating arcs have been already applied in practical combustors, further studies are needed to understand the characteristics of the interactive phenomena between the arc and flame. So far, there have been few fundamental studies on combustion assisted by rotating arc. Korolev et al. [25] demonstrated that a rotating arc is useful to extend flammability limits. Korolev et al. [26] later reported that a non-steady-state gas discharge process was observed in a rotating arc reactor for flame stabilization. Using more sophisticated experimental rotating arc apparatus and optical diagnostics, Ombrello et al. [9] revealed that the thermal effects of plasma are one reason for combustion enhancement. However, the information contained in these studies is insufficient to fully understand the interactive behavior of a rotating arc and a flame. For example, none of the previous studies investigate the effects of a flame on the generation or extinction of a rotating arc, which is one of the fundamental features of the plasma-flame interaction phenomena. In addition, NO_x emissions, which have long been a concern relating to combustion and which could increase due to highly dissociative reactions induced by an arc, have not been investigated in the previous studies. Therefore, further studies that characterize the fundamental features of flame interaction with a rotating arc are needed.

The objective of the present study is to extend the current understanding of the interactive phenomena between a rotating arc and a flame. In order to achieve this objective, a rotating arc and a premixed methane/air flame generated in a rotating arc reactor were investigated. In the early part of the study, a phenomenological observation of the flame and the rotating arc under different equivalence ratios was conducted. A special attention was paid to characterize how these different flame conditions affect the generation of the rotating arc. After the phenomenological observation, the product gases, CO_2, H_2, CO, C_2, C_3, and NO_x, were analyzed. Optical emission spectra (OES) were also detected to analyze the behavior of intermediate chemical species generated during the interaction process between the flame and the rotating arc.

Experimental Approach

The geometrical configuration of a rotating arc reactor is shown in Fig. 1. The rotating arc reactor consists of an inner electrode and an outer tube. The inner electrode is connected to the high voltage port. The outer tube is connected to the electrical ground. An example of practical diesel combustor, in which a technique of rotating arc is adopted, is also shown in Fig. 1. This combustor is installed in the exhaust line of a diesel engine, and is operated to regenerate a diesel particulate filter. As reported in elsewhere [4], the diesel flame is stabilized by the rotating arc under the harsh operating conditions of a diesel exhaust line, i.e., transiently varying low O_2 concentration (5–10%) and high mean combustion product velocity (20 m/s). The evolution of the rotating arc is schematically shown in Fig. 2. Initially, the arc is ignited at the shortest distance between the inner electrode and the outer
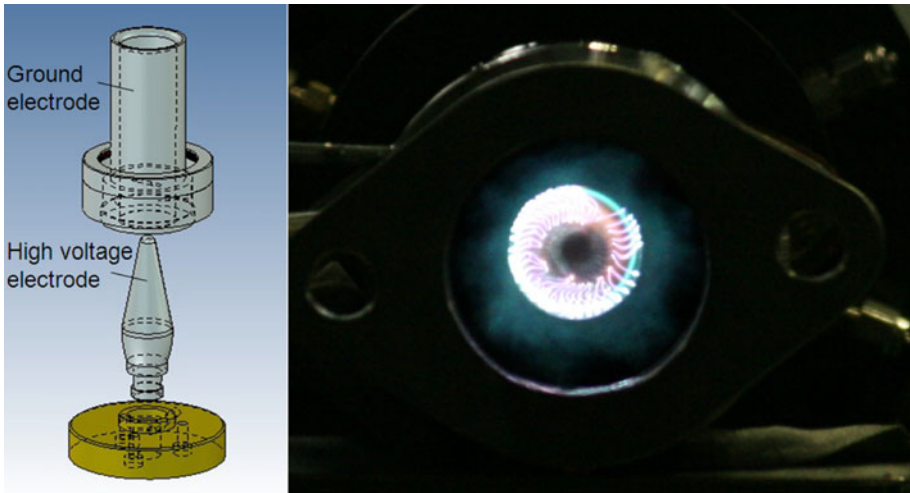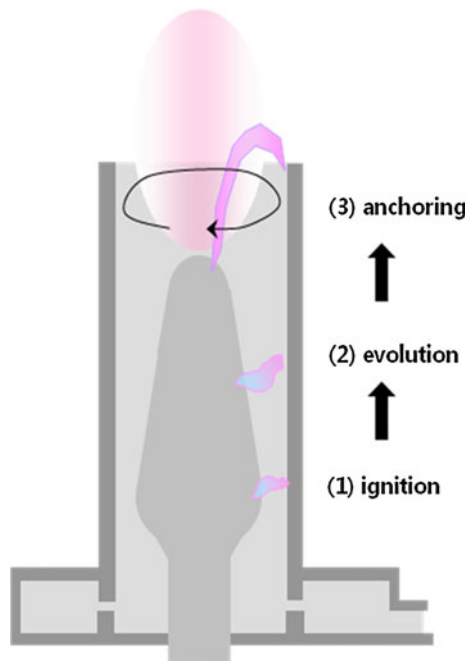
Fig. 1 Configuration of a rotating arc reactor consisting of an inner electrode and an outer tube (*left*), A diesel fuel combustor assisted by rotating arc (*right*). This diesel combustor is installed in a diesel exhaust line for regenerating diesel particulate filter [4]

Fig. 2 Development of a rotating arc: (**1**) ignition, (**2**) evolution, (**3**) anchoring

tube, which is located at the lower part of the reactor. After ignition, the arc is pushed upward and is rotated by tangentially injected gas flow motion. Eventually, the rotating arc is anchored between the upper part of the inner electrode and the edge of the outer tube, and the arc length reaches its maximum. However, depending on the input power and flow rates, the arc length could decrease in some cases. This would result in decreased peak

voltage and increased angular speed of the arc. These phenomena, along with different flame conditions, will be discussed in later sections. The present rotating arc is a three-dimensional version of a so-called gliding arc. The length and volume of a gliding arc are elongated and expanded by aerodynamic force. In the case of a gliding arc, the arc column can be expanded without further supply of electric power, resulting in a lower gas temperature as compared to a typical discharged arc. Because of this, gliding arcs are classified as non-equilibrium plasma [19–24], and can effectively generate chemically active species, although the roles of these species and the heat generated by gliding and rotating arcs in chemical processes are still being debated [12, 18, 27].

Figure 3 shows a schematic drawing of the test apparatus used in this study. It consists of a rotating arc reactor, power supply, gas supply, and gas detection system. Figure 4 shows typical voltage and current oscillograms of a rotating arc. An AC power supply (Dawonsys Co. AP CAF-2) was used, generating a peak voltage of 3–5 kV and peak current of 0.2–0.3 A. The frequency of AC power was fixed at 10 kHz. The power supply was capable of supplying a constant input power, regardless of the varied peak voltages. To detect the voltage applied to the electrodes, a high-voltage probe (1000:1, Tektronix, P6015A) was used. Currents were detected using a current probe (Tektronix, TCP202). The voltages and currents were recorded using a digital oscilloscope (Tektronix, TDS5054B). As shown in Fig. 3, CH_4 and air were supplied through a mass flow controller (MFC) (Brooks Co., 5850E, 5851E) and were premixed before being introduced into the reactor. The flow rates of CH_4 were varied and those of N_2 and O_2 were fixed to 15 L/min to change the equivalence ratio. In this way, any variation of total flow under different equivalence ratios was minimized. During most of the experiments, the electrical power input to the rotating arc reactor was fixed at 35 W. This power was estimated based on the
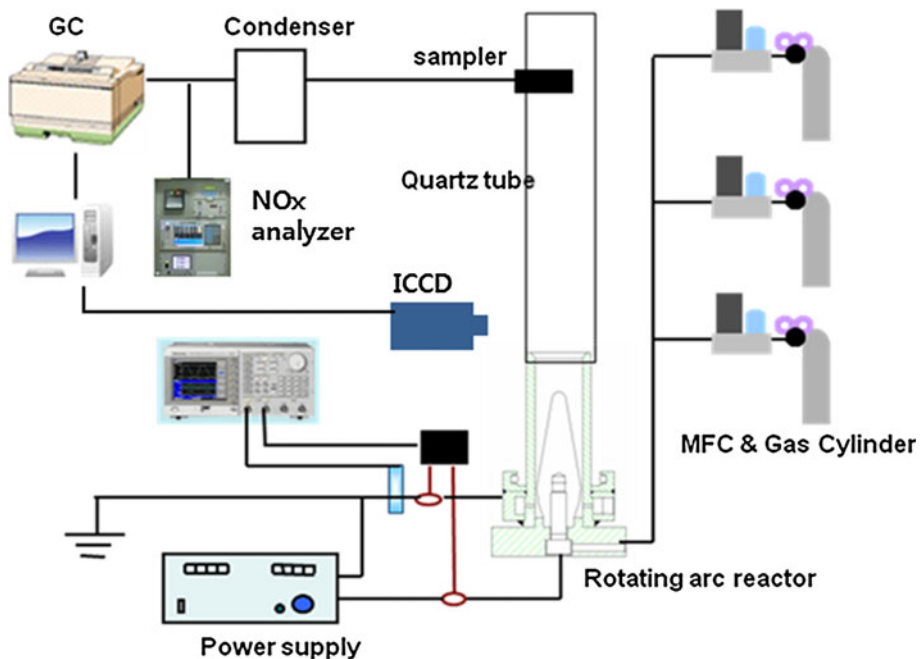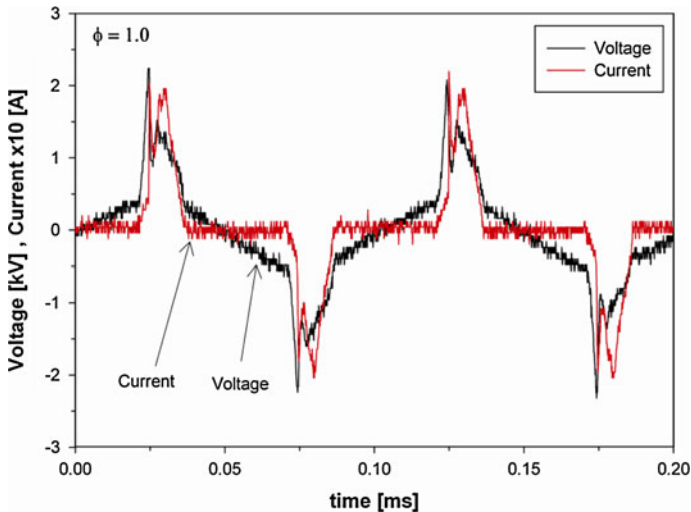

Fig. 3 Schematic of the test apparatus

Fig. 4 Oscillogram of voltage and current

voltage and current oscillograms. The electrical power supplied to the reactor was equivalent to approximately 3% of the total thermal power output produced by the stoichiometric methane flame. In the previous studies, the ratio of electrical power input to thermal power output varied in the range of 0.3–5% [2, 8, 26]. To generate a premixed flame, the outlet section of the rotating arc reactor was isolated from the surrounding air using a quartz tube that was 30 mm in diameter and 600 mm in length. A gas chromatograph (GC) (HP, G1530A) was used to detect the gases emitting from the rotating arc reactor, which were CH_4, C_2H_2, C_2H_4, C_2H_6, C_3H_6, C_3H_8, CO, CO_2, H_2, and O_2. NO and NO_2 were separately detected using a chemiluminescent NO_x analyzer (Signal Instrument, 4000vm). NO_x data was captured with 1 Hz of sampling rate and averaged for a minute for each realization and it does not need error bars for the data itself represents statistical value.

Optical emission spectra from the flame and arc were detected using an OES system consisting of a ultra-violet lens (Nikon), a monochromator (Spectro-Pro 500i, Acton Research Corporation), and an intensified charge-coupled device (ICCD, Princeton Instrument). ICCD camera is used for collecting the spatially resolved light emission from the discharge chamber. The delivered light is split by a monochromator of a wavelength range of 200–800 nm with an intensified multi-channel array detector (IRY). The spectral resolutions of 0.17 nm was obtained from the gratings of 150 g/mm. The spatial resolution, determined by the magnification factor of the lens and the pixel height of the ICCD, is 0.155 mm. To obtain the time-averaged spectrum, the long exposure time of 500 ms is used in all of the experiments together with 3 accumulations.

Result and Discussion

Figure 5 shows photographs of the flame and rotating arc at different equivalence ratios, Φ. Here, the exposure times of the camera for the top view and the side view are 1/500″ and 1/4″, respectively, and the input electrical power was fixed at 35 W. The figure shows that
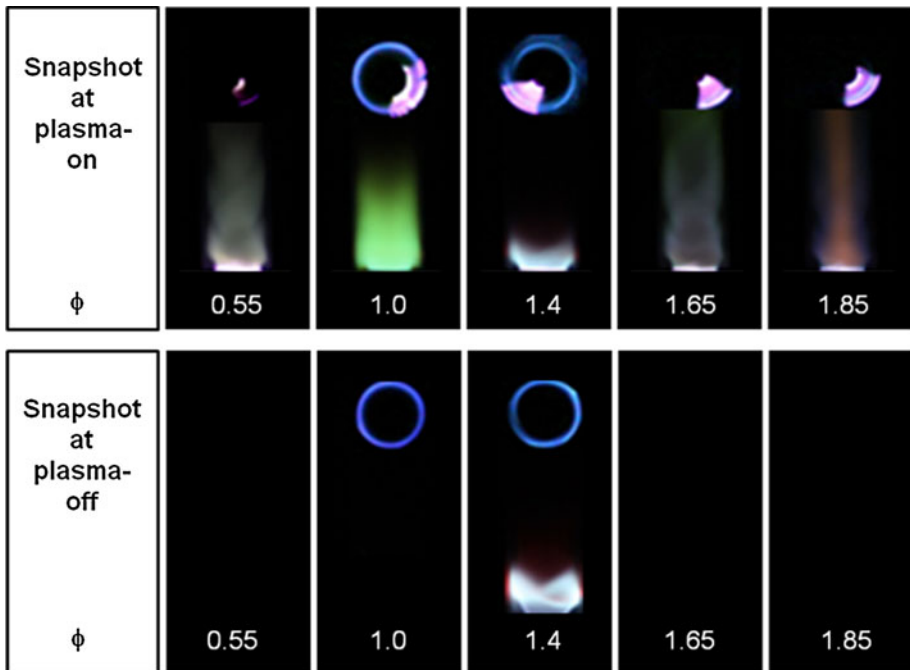
Fig. 5 Side and top views of the flame and rotating arc. Input electrical power: 35 W, Exposure time: side view, 1/4″; top view, 1/500″, In the case of plasma off at $\Phi = 0.55$, 1.65, and 1.85, flame is also blown off

the behavior of the flame—the colors, shapes, and extinction conditions of the flame—changed in the presence of the rotating arc. More interestingly, the behavior of the rotating arc was also affected by the flame conditions. As shown in Fig. 5, the arc length and the angular speed, which are closely related to the generation/extinction mechanism of the rotating arc, differed as Φ varied. These interactive phenomena between the flame and the rotating arc are discussed in detail in the following section.

Observation of the Flame Affected by the Rotating Arc

One noticeable change in the flame was its stabilization aided by the rotating arc. For an example, when $\Phi = 1.85$ and with 35 W of input power, the long and sooty flame shown in Fig. 5 was observed. Here, the flame was oscillating. This long and oscillating flame turned into a short and stabilized flame when the electrical power input increased, as shown in Fig. 6. The decrease of flame length caused by the rotating arc was also observed with $\Phi = 1.4$ condition, as shown in Fig. 5. The reason for the decreased flame length is that the methane oxidation process is accelerated by the rotating arc. In addition to flame stabilization, the rotating arc resulted in an extended flammability limit. As shown in Fig. 5, when the rotating arc was off, flames were extinguished under the fuel rich and lean conditions, e.g., $\Phi = 1.65$, 1.85, and 0.55. However, when the rotating arc was on, visible flames were observed under the same fuel rich and lean conditions. The above tests clearly demonstrated that a rotating arc is a convenient means to stabilize a flame oscillation and to extend flammability limits. In these tests, flames were controlled by simply controlling the electrical power input without varying geometrical configurations. Therefore, the present
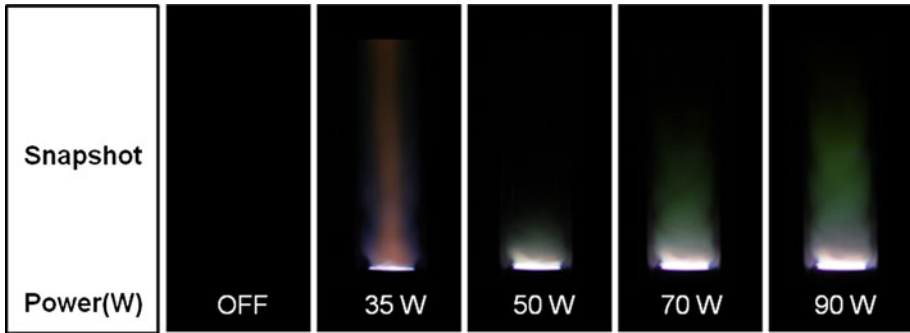
Fig. 6 Different flame shapes at different electrical power inputs; $\phi = 1.85$
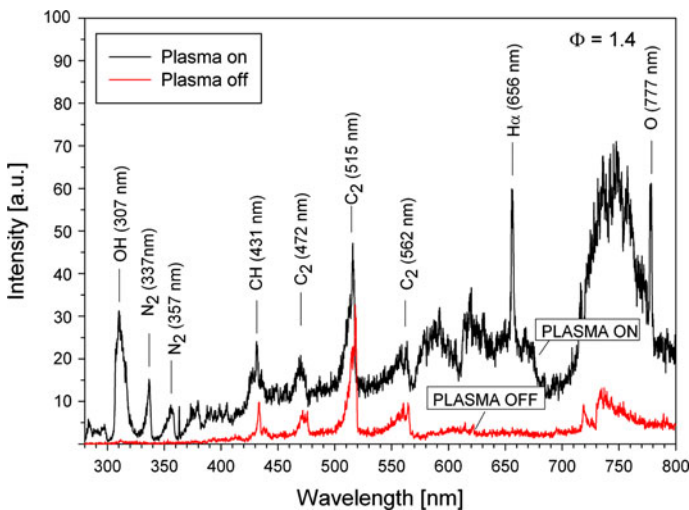

Fig. 7 Optical spectrum detected at $\Phi = 1.4$ and at 1–2 mm above the exit of the reactor. P = 35 W, Four sub-sections are combined for overall OES data (280–400, 400–550, 550–700, 700–800 nm)

flammability limit can be further extended when the geometrical configurations of reactors are optimized.

Figure 7 shows the OES at $\Phi = 1.4$, which was detected 1–2 mm above the reactor's exit. The spectral peak for OH ($A^2\Sigma^+ - X^2\Pi$, 306.4 nm), CH ($A^2\Delta - X^2\Pi$, 431 nm), and C_2 Swan band system was detected. These are the well-known spectral peaks detected in typical hydrocarbon flames. When the rotating arc was on, strong peaks for the N_2 ($C^3\Pi_u$– $B^3\Pi_g$, 337 nm, 357 nm), H_α (656 nm), and O atom (777 nm) were also observed. Detection of N_2 $C^3\Pi_u$–$B^3\Pi_g$ system means that some of energetic electrons generated by the rotating arc are higher than 11 eV [28], which is high enough to initiate plasma chemistry, such as electron impact dissociation of CH_4 and O_2. As discussed by Chintala et al. [7] and Adamovich et al. [10], plasma chemistry involved with the excited N_2 molecule, H_α and O atoms leads to favorable effects on flame, such as flame stabilization and reducing ignition delay time. Therefore, one can expect that these intermediate chemicals play a role to stabilize the flame and extend the flammability limits, as shown in Figs. 5 and 6.
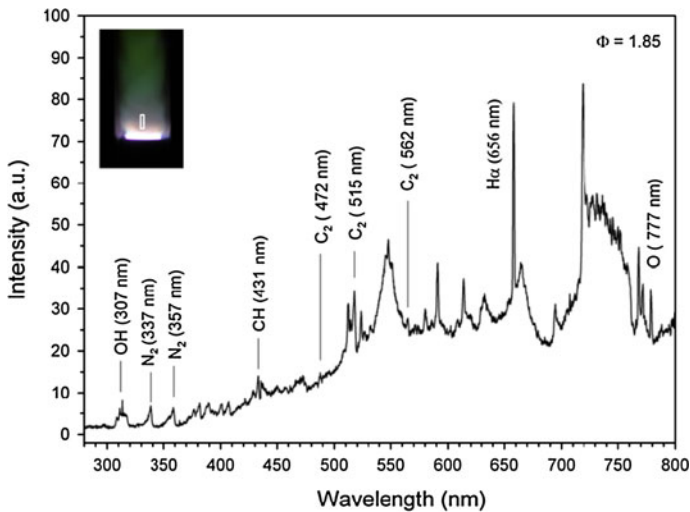
Fig. 8 OES obtained by integrating mathematically over the specific region represented by the rectangular. $\Phi = 1.85$ and input power = 70 W

One of the critical parameters to affect the OES is the height of the detection. First of all, unlike the OES detected at the exit of the reactor, shown in Fig. 7, the OES of the downstream are too weak to be identified. Such relatively weak OES is attributed to the fact that the arc, which generates high temperature and intermediate chemical species abundantly, does not exist in the downstream of the reactor. In order to check the weak OES of the downstream, the emission intensities were mathematically integrated over a specific region. Figure 8 shows an example of the integrated OES over a specific region. Here, the actual heights of this detection region are 11–31 mm above the exit. One noticeable difference between the OES of the downstream (Fig. 8) and the OES at the exit (Fig. 7) is that the identified peaks in the downstream, such as the peaks for the excited N_2, H_α, O, OH, C_2, are significantly reduced, compared to the emission continuum with a maximum around 550 nm. Similar emission continuum detected from a flame interacted with plasma has been reported by Vincent-Randonnier et al. [29]. They reported that this emission continuum generated by plasma is shown in the ranges between 450 and 800 nm and is intensified in the presence of flame. As shown in Fig. 9, the emission continuum is also detected from the downstream of the stoichiometric flame. The figure shows that the typical intermediate chemicals of hydrocarbon flames, such as CH, C_2, and CN, are not detected in the downstream. This indicates that green color emission observed at the downstream of the stoichiometric flame (Fig. 5) is not attributed to C_2 Swan band system that typically generates green flames under fuel rich condition.

Observation of the Rotating Arc Modified by Flame

Thus far, the effects of flame on plasma generation or extinction have been little explored compared to the effects of plasma on flame. In this study, the arc generation affected by the flame was clearly observed and characterized with the parameters of peak voltage and the equivalence ratio, Φ. As shown in Fig. 5, the length and angular speed of the rotating arc varies with respect to Φ. Under fuel rich and lean conditions, the rotating arc was pushed
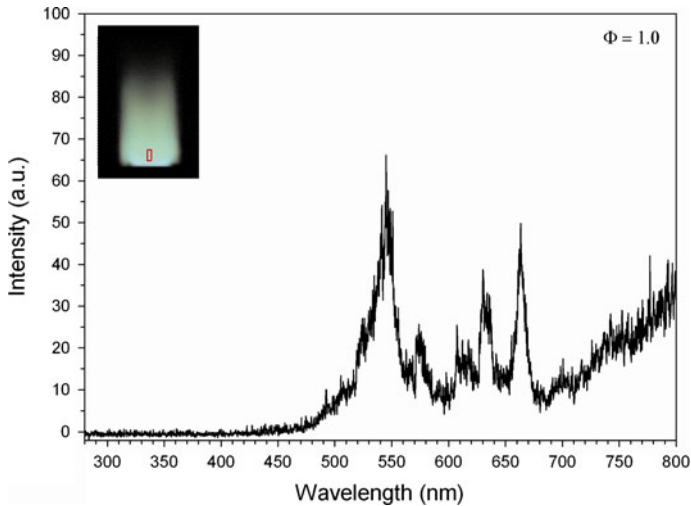
Fig. 9 OES obtained by integrating the weak emissions from the downstream of the stoichiometry flame with rotating arc, input power: 35 W. Visible image for this OES is shown in Fig. 5

upward and extended out from the reactor. The very bright arc region, which ended 3–4 mm above the reactor exit, was observable from the side. However, as Φ approached the stoichiometric condition, the arc tended to stay in the lower part of the reactor and was not observable from the side. The arc lengths were relatively short, resulting in faster angular speed. Because this observation is an indication that plasma generation could be affected by the flame condition, further tests were conducted to characterize the arc length under different Φ conditions. In these tests, characteristics of the peak voltage were investigated instead of the arc length. Because measuring the length of a curvilinear arc is not easy, we characterized the peak voltage that increases as the arc length increases [24].

Figure 10 shows the peak voltages at different Φ conditions. As expected, the lowest peak voltage was obtained at $\Phi = 1.0$. Visual observation of the arc length also confirmed that the shortest arc length was observed at the same Φ condition. According to previous studies of modeling a gliding arc [22, 24], the arc length of a gliding arc is critically determined by the relative velocity between the arc and the surrounding gases. When the relative velocity is large, the enhanced heat and mass transfer from the arc to the surrounding gases results in a decreased conducting arc radius and increased arc resistance. Due to these changes, the arc tends to be extinguished before it elongates further. Although the generation and extinction mechanisms of the rotating arc in this study were not exactly the same as those of the gliding arc, the variations in arc length could be attributed to the relative velocity between the arc and the combustion product gases. Because the velocity of the product gases expanded by the combustion process should be maximized at $\Phi = 1.0$, there is a strong possibility that the most active heat and mass transfer occur at the stoichiometric condition. In addition, variation of gas species and temperatures during the combustion process could also affect arc characteristics [19]. In order to reveal the present arc generation/extinction mechanism in detail, the physical and electrical characteristics of the rotating arc should be identified, which is beyond the scope of this study.
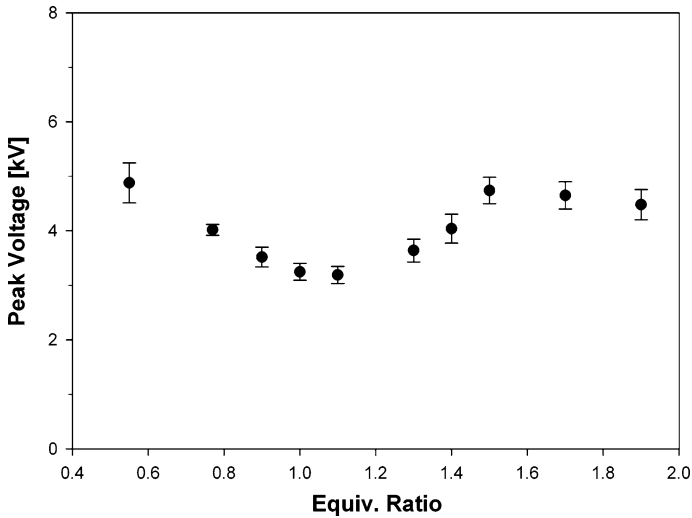
Fig. 10 Variation of the peak voltage at different equivalence ratios

Analysis of Product Gases

Figures 11,12, and 13 show the CH_4 conversion rate and selectivity of CO_2, H_2, CO, C_2, and C_3 hydrocarbons. Here, the selectivity of the gases is defined as follows:

$$\text{Conversion } CH_4 = \left(1 - \frac{\text{mole (product } CH_4)}{\text{mole (reactant } CH_4)} \right) \times 100$$

$$\text{Selectivity } CO_x = \frac{\text{mole (produced } CO_x)}{\text{mole (converted } CH_4)} \times 100$$

$$\text{Selectivity } H_2 = 0.5 \times \frac{\text{mole (produced } H_2)}{\text{mole (converted } CH_4)} \times 100$$

$$\text{Selectivity } C_xH_y = x \times \frac{\text{mole (produced } C_xH_y)}{\text{mole (converted } CH_4)} \times 100$$

Here, the reactions for the methane combustion and partial oxidation are the following;

$$CH_4 + 2O_2 + CO_2 + 2H_2O \,[\text{combustion}]$$
$$CH_4 + 1/2O_2 + CO + 2H_2 \,[\text{partial oxidation}]$$
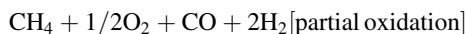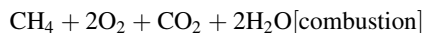
Because the rotating arc extends the flammability limit to an extremely fuel rich condition, part of the CH_4 conversion process under the rich fuel condition in this study was similar to the partial oxidation process that produces CO and H_2 as the major product gases, as shown in Fig. 12. In this test, as shown in Fig. 13, unlike a conventional partial oxidation process, noticeable amounts of C_2H_6, C_2H_4, and C_2H_2 were produced. This is an indication that the CH_4 conversion process in this study was incompletely terminated. As reported previously [12], to convert all the hydrocarbons to CO and H_2 using a rotating arc, the electrical power input density, defined as electrical power input divided by flow rate
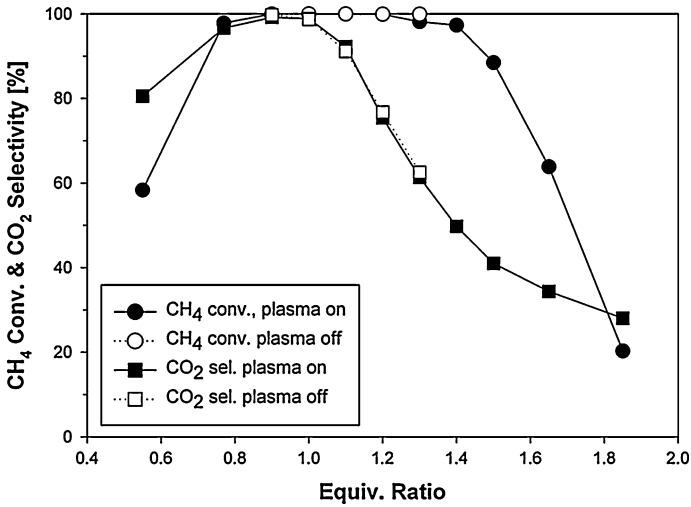
Fig. 11 CH_4 conversion rate and CO_2 selectivity

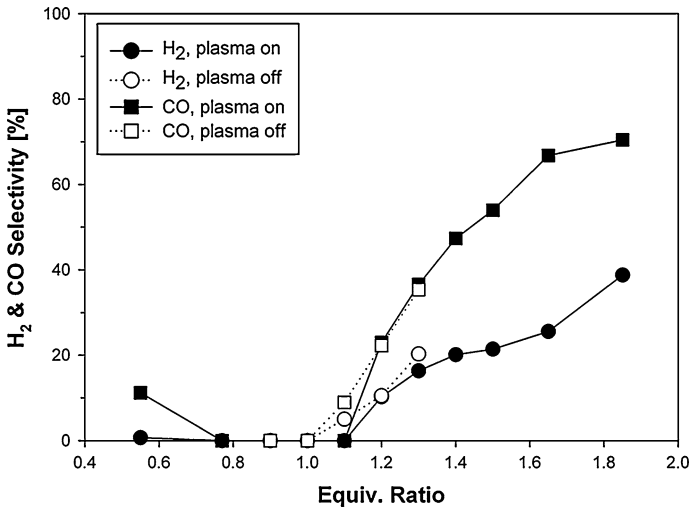**Fig. 12** H_2 and CO selectivity

[J/L], should be an order of magnitude higher than those in the present test. Therefore, the C_2 hydrocarbon emissions in the fuel rich conditions in this study are attributable to the small input power supplied to the reactor.

Another important characteristic of the CH_4 conversion is found around the stoichiometric conditions. As shown in Figs. 11 and 12, the amounts of the produced CO_2, CO, and H_2 around the stoichiometric conditions are not noticeably varied in the presence of the rotating arc. This implies that the rotating arc in this study does not significantly affect the major product gases of the combustion process. The reason for the production of similar major product gases can be explained by the relatively small input electrical energy. The electrical input energy in this study was small, equivalent to only 3% of the heat
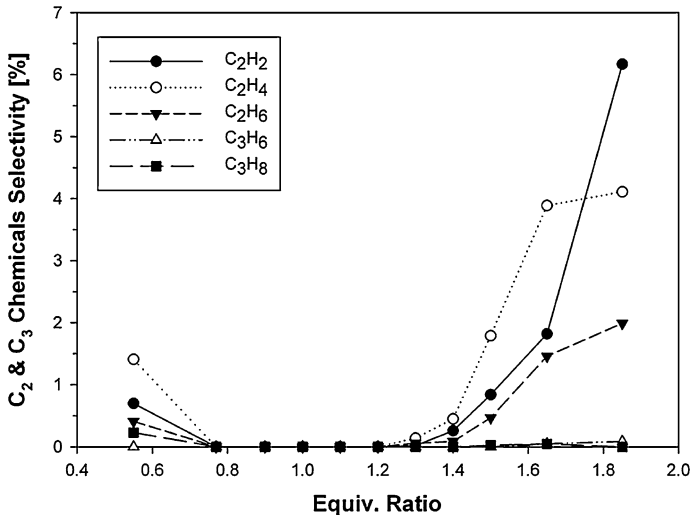
Fig. 13 C_2 and C_3 hydrocarbons

energy released from the stoichiometric combustion process. Therefore, the analysis of the product gases revealed that the arc energy consumed was not sufficiently high to control the selectivity of major species, but was sufficiently high to initiate and sustain the CH_4 conversion process under extremely fuel lean and rich conditions.

As discussed above, the rotating arc in this study did not control the major product gases such as CO_2, CO, and H_2. However, emission of minor species like NO_x (NO and NO_2) was significantly affected by the rotating arc. As shown in Fig. 14, the concentrations of NO_x generated by the rotating arc were higher than those generated by combustion by an order of magnitude. In addition, the equivalence ratio (Φ) of the highest NO_x concentration is different depending on the plasma condition. When the plasma is on, the highest NO_x concentration is obtained at the smallest equivalence ratio condition, i.e. the leanest fuel condition. In contrast, when the plasma is off, the highest NO_x concentration is obtained at $\Phi = 1.0$. In general, NO emitted from hydrocarbon-air flames is mostly generated through the following reactions, known as thermal or Zeldovich mechanism [30].

$$O + N_2 \rightarrow NO + N$$
$$N + O_2 \rightarrow NO + O$$
$$N + OH \rightarrow NO + H$$
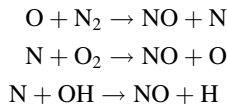
Here, N and O radicals are generated from N_2 and O_2 molecules, respectively. Since the most active thermal mechanism occurs at the highest temperature condition, the stoichiometric condition, $\Phi = 1.0$, at which the flame temperature closely approaches the maximum adiabatic flame temperature, is the most favorable condition for NO formation. This is the reason why the highest NO_x concentration is obtained at $\Phi = 1.0$, as shown in Fig. 14, when the plasma is off. When the plasma is on, however, since the thermal environment needed for NO formation is already provided by the arc, the role of the heat from the combustion process is not critical any more. In this case, the concentration of O_2 molecule to generate O radical plays more important role in NO formation. Therefore, the highest NO_x concentration is obtained at the leanest fuel condition.
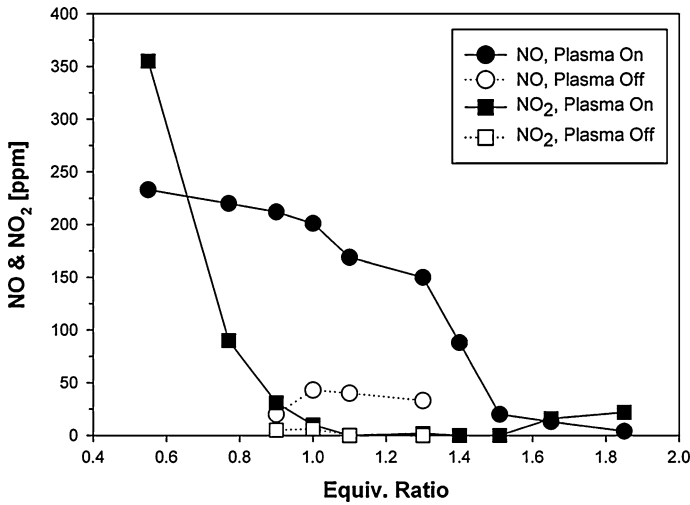
Fig. 14 Variation of NO$_x$ and the equivalence ratio

Figure 14 shows the abrupt decrease in NO and NO$_2$ concentrations starting at $\Phi = 1.3$ and 0.55, respectively. The decrease in the NO concentration starting in the rich fuel condition can be attributed to the lack of O$_2$ molecules and the selective non-catalytic reduction of NO with hydrocarbons, H$_2$, and CO. One of the most likely reasons for the abrupt decrease in NO$_2$ when approaching the stoichiometric condition is the following reductive reactions of NO$_2$ to NO with O and H radicals in a high-temperature environment [30].

$$NO_2 + H_2 \rightarrow NO + OH$$
$$NO_2 + O \rightarrow NO + O_2$$
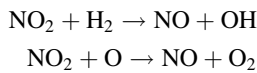
In many previous studies on flame affected by plasma, NO$_x$ emissions generated by plasma have not been discussed. However, as shown in Fig. 14, the present study suggests that NO$_x$ generated by plasma under fuel lean conditions could be a serious factor preventing the application of plasma in the combustion process. Therefore, careful design considerations regarding NO$_x$ emissions are needed when plasma is applied to practical combustors.

Conclusion

Characteristics of a premixed methane flame generated with a rotating arc are investigated. In the early part of the study, phenomenological observations of the flame and arc are carried out, confirming that the rotating arc plays a role to stabilize the flame and extend the flammability limit. The observation also showed that the important features of the rotating arc—arc length, angular speed, peak voltages—are affected by the flame conditions, i.e. equivalence ratios. These observations reveal that both of the flame and the rotating arc are interactively affected. The OES tests indicated that the intermediate chemicals generated by rotating arc, such as excited N$_2$, O and H, are relatively abundant only in the arc and the region which is close to the arc. In the downstream of the reactor, which is away from the arc, emission intensity for the above intermediate chemicals decreases significantly. The OES tests also showed that emission continuum with a

maximum around 550 nm appeared in the presence of the rotating arc, which could result in green color flame under the fuel rich conditions. Although the shape and the optical emissions of the flames are significantly affected by the rotating arc, the gas analysis revealed that the major gas products, such as CO_2, CO, H_2, are not significantly changed. However, gas analysis showed that NO_x emissions can significantly increase in the presence of a rotating arc. A rotating arc can generate meaningful amounts of N and O radicals without the heat released from a flame; therefore, the highest NO_x concentration was found under fuel lean conditions. The present test of NO_x emissions suggests that careful consideration is necessary in the investigation and practical application of rotating arcs.

References

1. Horng R-F, Wen C-S, Liauh C-T, Chao Y, Huang C-T (2008) Int J Hydrogen Energy 33:7619–7629
2. Pilla G, Galley D, Lacoste DA, Lacas F, Veynante D, Laux CO (2006) IEEE Trans Plasma Sci 34:2471–2477
3. Kim W, Mungal MG, Cappelli MA (2010) Combust Flame 157:374–383
4. Lee DH, Kim K-T, Cha MS, Lee JO, Song Y-H, Cho H, Kim Y-S, Song Y, Jee T (2009) SAE Paper 2009, 09SFL-0065
5. Mintusov E, Serdyuchenko A, Choi I, Lempert WR, Adamovich IV (2009) Proceed Combust Inst 32:3181–3188
6. Kim Y, Ferreri VW, Rosocha LA, Anderson GK, Abbate S, Kim K (2006) IEEE Trans Plasma Sci 34:2532–2536
7. Chintala N, Meyer R, Hicks A, Bao A, Rich JW, Lempert WR, Adamovich IVJ (2005) Propuls Power 21:1–7
8. Starikovskaia SMJ (2006) Phys D Appl Phys 39:R265–R299
9. Ombrello T, Won SH, Ju Y, Williams S (2010) Combust Flame 157:1916–1928
10. Adamovich IV, Choi I, Jiang N, Kim J-H, Keshav S, Lempert WR, Mintusov E, Nishihara M, Samimy M, Uddi M (2009) Plasma Sour Sci Technol 18:034018
11. Ombrello T, Qin X, Ju Y, Gutsol A, Fridman A, Carter C (2006) AIAA J 44:142–150
12. Lee DH, Kim KT, Cha MS, Song Y-H (2007) Proceed Combust Inst 31:3343–3351
13. Rollier J-D, Gonzalez-Anguilar J, Petipas G, Darmon A, Fulcheri L, Metkemeijer R (2008) Energy Fuels 22:556
14. Petipas G, Gonzalez-Anguilar J, Darmon A, Fulcheri L (2010) Energy Fuels 24:2607
15. Lebouvier A, Fresnet F, Fabry F, Boch V, Rohani V, Cauneau F, Fulcheri L (1034) Energy Fuels 2011:25
16. Rueangjitt N, Sreethawong T, Chavadej S, Sekiguchi H (2011) Plasma Chem Plasma Process 31:517
17. Lee DH, Kim K-T, Cha MS, Song Y-H (2010) Int J Hydrogen Energy 35:4668–4675
18. Lee DH, Kim K-T, Cha MS, Song Y-H (2010) Int J Hydrogen Energy 53:10967–10976
19. Fridman A, Nester S, Kennedy LA, Saveliev A, Mutaf-Yardimici O (1998) Progress Energy Combust Sci 25:211–231
20. Nassar H, Pellerin S, Musiol K, Martinie O, Pellerin N, Cormier J-MJ (2004) Phys D Appl Phys 37:1904–1916
21. Pellerin S, Cormier J-M, Richard F, Musiol K, Chapelle JJ (1996) Phys D Appl Phys 29:726–739
22. Pellerin S, Richard F, Chapelle J, Cormier J-M, Musiol KJ (2000) Phys D Appl Phys 33:2407–2419
23. Pellerin S, Cormier J-M, Richard F, Musol K, Chapelle J (1999) J Phys D Appl Phys 32:891
24. Richard F, Cormier J-M, Pellerin S, Chapelle JJ (1996) Appl Phys 79:2245–2250
25. Korolev YD, Matveev IB (2006) IEEE Trans Plasma Sci 34:2507–2513
26. Korolev Y, Frants OB, Landl NV, Geyman VG, Matveev IB (2009) IEEE Trans Plasma Sci 37:586–592
27. Benilov MS, Naidis GV (2006) Int J Hydrogen Energy 31:769–774
28. Spyrou N, Manassis CJ (1989) Phys D Appl Phys 22:120–128
29. Vincent RA, Larigaldie S, Magre P, Sabel'nikov V (2007) Plasma Sour Sci Technol 16:149–160
30. Turns SR (1996) An introduction to combustion. McGraw-Hill, New York